Neuron, Vol. 28, 345–356, May, 2000, Copyright ©2000 by Cell Press

rpm-1, A Conserved Neuronal Gene that Regulates Targeting and Synaptogenesis in *C. elegans*

Anneliese M. Schaefer, Gayla D. Hadwiger, and Michael L. Nonet*
Department of Anatomy and Neurobiology
Washington University School of Medicine
Saint Louis, Missouri 63110

Summary

Little is known of mechanisms regulating presynaptic differentiation. We identified *rpm-1* in a screen for mutants with defects in patterning of a presynaptic marker at certain interneuronal synapses. The predicted RPM-1 protein contains zinc binding, RCC1, and other conserved motifs. In *rpm-1* mutants, mechanosensory neurons fail to accumulate tagged vesicles, retract synaptic branches, and ectopically extend axons. Some motor neurons branch and overgrow; others show altered synaptic organization. Expression of RPM-1 in the presynaptic mechanosensory neurons is sufficient to rescue phenotypes in these cells. Certain *rpm-1* phenotypes are temperature sensitive, revealing that RPM-1 function can be bypassed by maintaining mutants at the permissive temperature at stages commensurate with synapse formation in wild-type animals. These results indicate that RPM-1 functions cell autonomously during synaptogenesis to regulate neuronal morphology.

Introduction

The culmination of synaptogenesis is the differentiation of the pre- and postsynaptic cells. Presynaptic differentiation includes transition of a dynamic, motile growth cone to a stable structure. Components that enable regulated secretion of neurotransmitter, such as Ca^{2+} channels and synaptic vesicles containing transmitter, are localized to release sites (Hall and Sanes, 1993). On the postsynaptic side, receptors and signal transduction machinery are assembled, poised to detect chemical transmission (Sanes, 1997; Craig, 1998).

Little is known of the cellular and molecular mechanisms in the presynaptic cell that underlie establishment of synaptic architecture (Sanes and Lichtman, 1999). Extracellular molecules, such as laminin β2 or FGF2, can promote specialization of the vertebrate neuromuscular junction (NMJ) (Dai and Peng, 1995; Noakes et al., 1995); likewise, laminin β2 can trigger assembly of synaptic components in chick ciliary ganglia (Son et al., 1999). Neuronal agrin facilitates presynaptic differentiation at the NMJ; however, this mechanism is likely indirect, involving retrograde signaling from muscle (Burgess et al., 1999). An increase in Ca^{2+} levels also may regulate cytoskeletal rearrangements that accompany synaptogenesis (Dai and Peng, 1996). It is unknown how the presynaptic cell implements these extracellular signals in downstream events of synaptic differentiation. Nevertheless, it is widely held that these processes are conserved across species (Hall and Sanes, 1993; Garrity and Zipursky, 1995).

We have used the genetic model organism *C. elegans* to study questions of synaptogenesis. The cell lineage (Sulston and Horvitz, 1977; Sulston et al., 1983) and circuitry (White et al., 1986) of all 302 neurons of the adult *C. elegans* nervous system have been defined. Our focus is the mechanosensory touch circuit, which has been well characterized at both the molecular and cellular levels (Chalfie et al., 1985; Chalfie and Au, 1989; Mitani et al., 1993). Moreover, the mechanosensory neurons form neuron–neuron synapses, providing an opportunity to complement studies of presynaptic differentiation at the NMJ. By tagging synaptic vesicles in these cells with the vital marker green fluorescent protein (GFP) (Chalfie et al., 1994), we generated living animals with a stereotypic and heritable fluorescence pattern (Nonet, 1999). In screening for mutations that alter this characteristic pattern, we have identified and describe here the cloning of a conserved neuronal gene, *rpm-1* (regulator of presynaptic morphology). The *rpm-1* gene was cloned independently by Zhen et al. (2000 [this issue of *Neuron*]), screening for alterations of synaptic patterning in a subset of motor neurons. Likewise, Wan et al. (2000 [this issue of *Neuron*]) cloned the *Drosophila* RPM-1 homolog in a functional and anatomical screen for synaptic growth at the NMJ.

The RPM-1 protein and its human and fly orthologs contain several motifs. Among these are an RCC1 domain, which is suggestive of exchange factor activity for a small GTPase, as well as B-box and RING zinc finger domains, which connote protein–protein interactions. In *C. elegans*, the *rpm-1* gene is expressed in most if not all neuronal cell types. Depending on cell type, loss of function mutations disrupt localization of synaptic vesicles and cause retraction of synaptic branches away from the target, generate ectopic axonal branching, or alter patterning of presynaptic specializations. We show that expression of the wild-type RPM-1 protein in the presynaptic mechanosensory neurons can rescue the mutant phenotypes in these neurons, demonstrating that RPM-1 can act cell autonomously. Further, certain phenotypes are temperature sensitive in both *rpm-1* alleles recovered in our screen. Assaying synapse formation by the posterior mechanosensory neurons, we present temperature shift data that reveal the discrete developmental window when animals are most sensitive to loss of RPM-1 function. This window corresponds to the time of synaptogenesis in wild-type animals. Consistent with these data, we propose that RPM-1 is part of a complex regulatory mechanism of presynaptic differentiation.

Results

Synaptic Vesicle Localization Is Altered in *rpm-1* Mutants

We previously have described the tool SNB-1::GFP, which permits visualization of presynaptic specializa-

*To whom correspondence should be addressed (e-mail: nonetm@thalamus.wustl.edu).

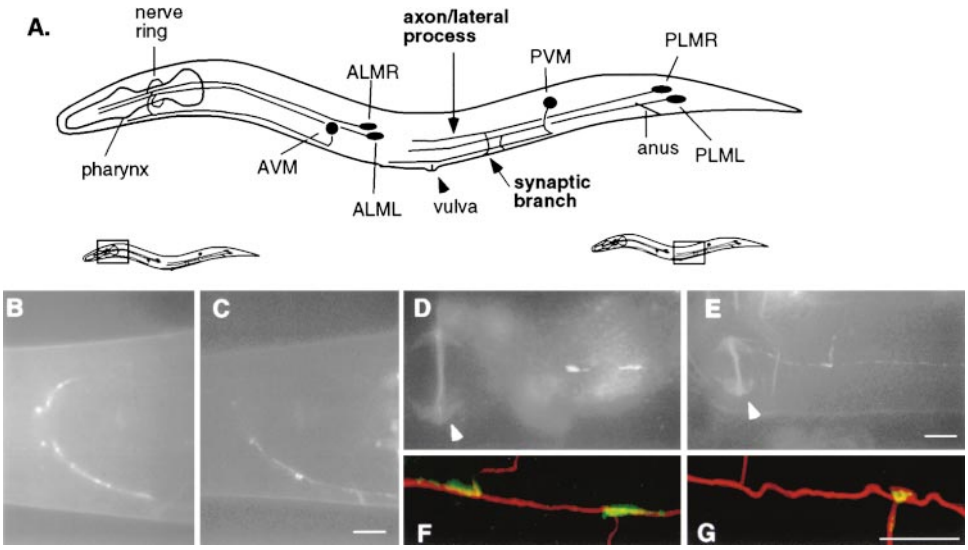

Figure 1. Synaptic Vesicles Fail to Localize in Mechanosensory Neurons in *rpm-1* Mutants

(A) Schematic of the six mechanosensory neurons in *C. elegans*. Anterior is to the left, and ventral is down.

(B–E) Epifluorescence images showing the pattern of SNB-1::GFP in single focal planes. Anterior is to the left. Lateral views showing more abundant puncta in the nerve ring of a *jsIs37* animal (B) than in a *jsIs37 rpm-1(js317)* mutant (C). Ventral view showing a *jsIs37* animal with two patches of fluorescence in the VNC, posterior to the vulva (D); ventral view of a *jsIs37 rpm-1(js317)* mutant lacking such an accumulation of tagged synaptic vesicles, despite presence of a synaptic branch (E). The signal in (E) has been enhanced to show the synaptic branch and reveals diffuse puncta in the VNC, which we observe in mutant and in wild type. These puncta may correspond to the PVM axon, which runs along this region of the VNC (see [A]). The synaptic branches in (D) are out of the plane of focus. An arrowhead marks the vulva in (D) and (E).

(F and G) Confocal images showing immunostaining of anti-GFP (green) and anti-MEC-7 (red), which labels microtubules unique to the mechanosensory neurons. The two GFP accumulations (green) in *jsIs37* are at the intersection of the synaptic branches (red) and the VNC (F). In a *jsIs37 rpm-1(js317)* mutant, both synaptic branches are present; an atypically small accumulation of GFP-tagged synaptic vesicles is present in one of the two branches (G).

Scale bars, 10 μm.

tions (Nonet, 1999). The SNB-1::GFP DNA construct is designed to fuse GFP to the integral membrane protein synaptobrevin (SNB-1), which is found on synaptic vesicles. In the stable strain *jsIs37*, SNB-1::GFP is expressed under control of the mechanosensory neuron-specific promoter $_{p}$*mec-7* (Hamelin et al., 1992; Mitani et al., 1993); hence, we label only those interneuronal synapses formed by the six mechanosensory cells (Figure 1A). *jsIs37* animals respond to touch, behave, and develop like wild type (Nonet, 1999). The pattern of vesicle-tagged fluorescence in these integrants is stereotypical and predicted. Fluorescence accumulations appear in the nerve ring and in the ventral nerve cord (VNC) neuropil, corresponding to glutamatergic synapses made by the mechanosensory neurons (White et al., 1986). Specifically, puncta decorating the nerve ring (Figure 1B) correlate to en passant synapses made by the anterior mechanosensory cells ALM and AVM. Along the VNC, 90% of animals present two patches of fluorescence (Figure 1D); the remaining 10% have one patch (n = 108). These patches arise during the first larval stage, L1. They are situated where the PLM neurons have extended from each axon a branch, or "synaptic branch" (Chalfie et al., 1985), that fasciculates with the VNC (Figures 1A and 1F). In the VNC, PLM forms 11 closely spaced en passant synapses onto 4 neuronal cell types (White et al., 1986). Our laser ablation analyses indicate that each of these fluorescent patches derives from each of the bilateral neurons (data not shown). Thus, each patch represents multiple synapses.

To identify molecules that regulate synaptogenesis, we screened for mutated genes that alter this stereotypical pattern of presynaptic fluorescence in *jsIs37* animals (see Experimental Procedures). From this screen, we identified the *rpm-1* gene. The two *rpm-1* alleles, *js317* and *js410*, are recessive and have phenotypically similar GFP and behavioral phenotypes. Specifically, *rpm-1* animals never display the two fluorescent patches in the VNC (Figure 1E) and are missing several puncta in the nerve ring neuropil (Figure 1C). Observing staged populations, these phenotypes persist throughout development (n = 142); therefore, the *rpm-1* defect is unlikely to have been caused by failure to maintain vesicles at the synapse.

The *rpm-1* defect does not alter differentiation of the mechanosensory neurons. We still observe *mec-7* (Figure 1E) and *mec-18* (Figures 2B, 2D, and 2F) promoter–specific expression. The neurons are labeled by the anti-MEC-7 antibody (Figure 1G), indicating that they likely contain the large diameter microtubules specific to these cells. Cell bodies are positioned normally (Figures 2D and 2F). Mechanosensory cell processes are fully extended, albeit often too far (see below).

The *rpm-1* phenotype does not reflect a general deficit in targeting to the appropriate target region. Despite the failure to accumulate synaptic vesicles, we often observe the normal pattern of synaptic branch targeting in *rpm-1* mutants (Figure 1G). During development, most (59%, n = 54) *rpm-1* mutant animals extend a synaptic branch from at least one of the bilateral axons. Nevertheless, branches appear to retract later in development (see below). Our data indicate that, for those neurons

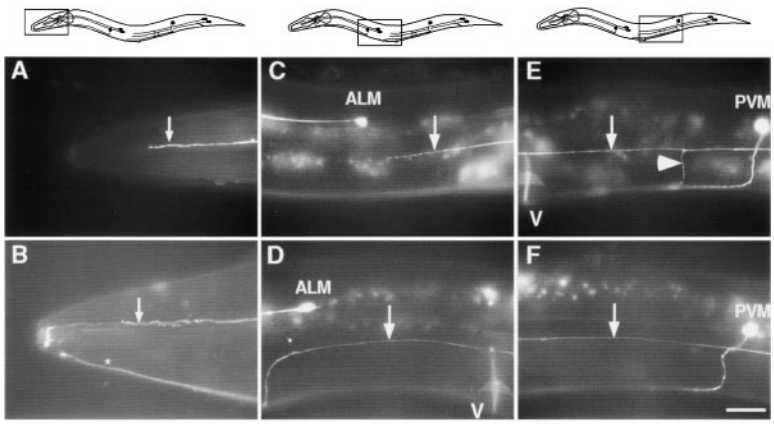

Figure 2. Altered Morphology in *rpm-1* Mechanosensory Neurons

Cytoplasmic GFP is expressed in the mechanosensory neurons using $_p$*mec-18*::GFP ("*uIs25*"). Epifluorescence images showing GFP expressed throughout the mechanosensory neurons in *uIs25* animals (A, C, and E) and *uIs25; rpm-1* mutants (B, D, and F). All images show lateral views and a single focal plane. Anterior is to the left, and ventral is down.

(A and B) The ALM axon (small arrow) stops just posterior to the nose in wild type (A) but overgrows and loops back in an *rpm-1* mutant (B). The AVM axon (asterisk, [B]) shows normal morphology in this mutant animal.

(C and D) The PLM axon (large arrow) stops near the ALM soma in wild type (C) but overgrows and targets ventrally in an *rpm-1* mutant (D).

(E and F) In a wild-type animal (E), a synaptic branch (arrowhead) forks from the PLM axon (large arrow) and is situated between the PVM soma and the vulva (V). No synaptic branch is visible in this *rpm-1* mutant adult (F).

Scale bar, 10 μm.

that extend a stable synaptic branch to the VNC, synapses either do not form or lack the normal complement of synaptic vesicles.

Defects in *rpm-1* mutants are not the result of defects in postsynaptic cell differentiation. The postsynaptic neurons are AVA, AVD, DVA, and PDE (White et al., 1986). Laser ablation of AVA and AVD in wild-type animals generates an uncoordinated phenotype, consistent with the role of these interneurons in mediating locomotion (Chalfie et al., 1985). In contrast, *rpm-1* mutants move well. Moreover, expression of GFP throughout AVA and AVD, as well as several other cell types, using the *glr-1* promoter (Hart et al., 1995; Maricq et al., 1995) indicates normal morphology of these postsynaptic neurons (data not shown).

rpm-1 mutants are mildly dumpy (Dpy) and have a subtle phenotype of retaining eggs (Egl); otherwise, they do not display any gross behavioral phenotypes. They respond to touch, consistent with the observation that chemical synapses made by *C. elegans* mechanosensory neurons are not required for the touch response (Chalfie et al., 1985). Although morphology of different classes of motor neurons is altered in *rpm-1* mutants (see below), these animals move well, confirming that circuitry of the interneurons and motor neurons that mediate the characteristic sinusoidal movement is fundamentally intact. Male animals mate, indicating proper function and wiring of the sensory neurons known to regulate this complex behavior (reviewed by Emmons and Sternberg, 1997).

Mechanosensory Cell Targeting Is Altered in *rpm-1* Mutants

In wild-type animals, PLM neurons differentiate and complete most axonal outgrowth in the embryo (Sulston et al., 1983). Just after hatching, these neurons have a process extending to the midbody region, adjacent to the ALM soma. While this axon grows in length as the animal grows during development, the end of the axon relative to the ALM soma is maintained (Figure 2C, arrow). Prior ultrastructural analysis indicates that there are no synaptic specializations at this ending or along the lateral process (White et al., 1986). Instead, the PLM synapses are found along the synaptic branch (Figure 2E, arrowhead), which first appears at approximately the mid-L1 stage (Figure 3). Thus, PLM synaptogenesis is temporally distinct from axonal outgrowth.

In *rpm-1* mutants, PLM morphology initially appears normal. In L1 animals, the cell bodies are appropriately situated, and lateral processes extend to the midbody region. However, our analyses of staged populations of animals indicate that extension and stabilization of the synaptic branch are disrupted in *rpm-1* mutants. Those branches that are observed appear slightly later in development than the targeting of branches in wild type (Figure 3). The average number of synaptic branches per mutant animal increases from 0.1 ($n = 57$ animals) to 0.9 ($n = 58$ animals); nevertheless, it never approaches the wild-type standard of two synaptic branches per animal, i.e., one branch from each bilateral PLM axon (Figure 3). Even those animals that show appropriate targeting to the VNC likely retract those branches, as the average number of branches per animal declines throughout later larval stages to 0.5 ($n = 86$ animals) (Figure 2F).

In addition to defects in synaptic branch morphology, we also observe ectopic growth and targeting. Anterior touch neurons often grow past their normal point of termination, then loop back (Figures 2A and 2B). As noted, morphology of the posterior PLM neurons is normal when *rpm-1* mutants first hatch, reflecting the normal quiescent stage of PLM axon outgrowth. However, during the mid-to-late L1 stage, PLM axons in most *rpm-1* animals grow past their normal stopping point (Figure 2D), usually extending toward, and fasciculating with, axon bundles in the VNC neuropil (Table 1). Unlike the synaptic branch, the ectopic axonal extension appears to be maintained throughout development (Figure 3), and the phenotype is completely penetrant in adults raised at 22.5°C (Table 1). Such aberrant growth, combined with the failure to properly localize synaptic vesicles, is consistent with a model whereby the neuron fails to form mature synapses at the appropriate time and place; as a consequence of retrograde signaling, the

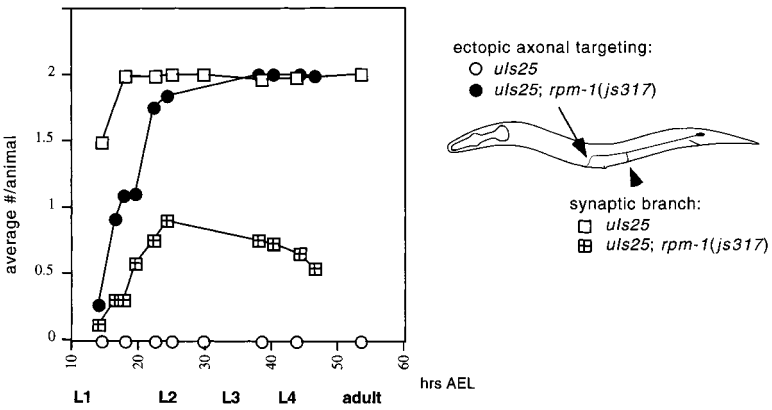

Figure 3. Comparative Development of *rpm-1* Branching Phenotypes

Populations of staged animals were raised at 22.5°C, and then each population was scored once for the presence of a synaptic branch and ectopic overgrowth of the PLM axon. For each time point, 41 to 86 animals were scored. The average number per animal is plotted as a function of hours after egg laying (AEL). Developmental stages are shown in bold.

neuron then generates ectopic targeting to the VNC (see Discussion).

Certain *rpm-1* phenotypes in the mechanosensory neurons depend on temperature. Accumulation of synaptic vesicles (see below) and stabilization of the synaptic branch are temperature sensitive. In adults that have been raised at 22.5°C, we observe a synaptic branch in 14% of the axons, whereas in animals that have been raised at 15°C, the number of synaptic branches observed increases 4-fold (Table 1). In contrast, the phenotype of ectopic branching from the end of the axon is not temperature sensitive; we observe altered axonal morphology in all animals raised at 22.5°C and in 98% of animals raised at 15°C (Table 1).

Temperature-Sensitive Window in Mutants Coincides with PLM Synaptogenesis in Wild Type

The accumulations of tagged synaptic vesicle fluorescence in the VNC are not present at the hatching of wild-type animals (Figure 4A). By the early second larval stage, however, most (103 of 114) animals have the two characteristic fluorescence patches. These patches are maintained throughout development, and their number and formation are not dependent on temperature: the average number of patches per animal is 1.90 when raised at 22.5°C (n = 108), and 1.97 when raised at 15°C (n = 105). On the other hand, the presence of patches in *rpm-1* animals shows temperature-sensitive variability. When the animals are raised at 22.5°C, we never observe the wild-type pattern of two patches (n = 142). Instead, almost all (130 of 142) animals lack fluorescence accumulations along the VNC; the remaining 12 of 142 show one patch of fluorescence. The calculated average number of patches per animal raised at 22.5°C is 0.08. In contrast, mutant animals raised at 15°C show greater fidelity in accumulating tagged synaptic vesicles. The majority (97 of 182) have at least one patch of fluorescence, and one quarter of these (24 of 97) show the wild-type pattern of two patches. The calculated average number of patches per animal is 0.66.

We next asked, during what particular stages in development, if any, must *rpm-1* mutants be at the permissive temperature in order to achieve this increase in tagged vesicle fluorescence? Animals were raised initially at

Table 1. Temperature-Sensitive Morphology in PLM Neurons

	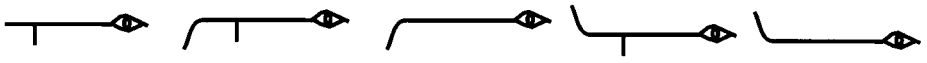					n
uIs25 22°	98	2	0	0	0	59
uIs25 15°	100	0	0	0	0	56
uIs25; rpm-1(js317) 22°	0	12	81	2	6	52
uIs25; rpm-1(js317) 15°	2	50	42	4	2	52

Morphologies observed for a single bilateral PLM neuron, using $_{p}$*mec-18*::GFP (*uIs25*). The cell is schematized as a cat eye–shaped soma, an axon that extends anteriorly from the soma, and a synaptic branch perpendicular to the axon, targeting ventrally. Animals were raised at the temperature indicated, then scored as adults for PLM morphology. The table identifies the percent of axons showing each morphology. Anterior is to the left, and ventral is down. Abbreviation: n, the number of animals examined for each genotype at the temperature indicated.

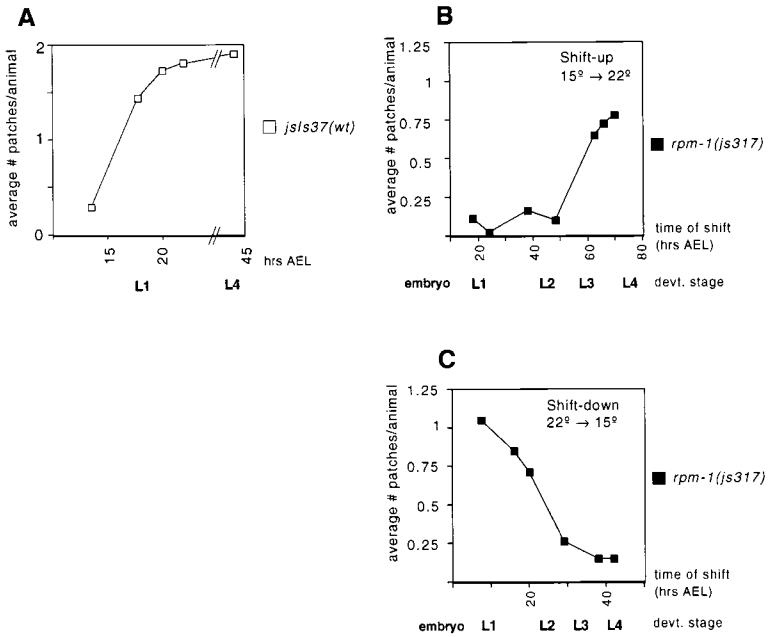

Figure 4. Temporal Window of *rpm-1* Temperature Sensitivity Corresponds to PLM Synaptogenesis in Wild-Type Animals

(A) *jsIs37* animals develop the characteristic two patches of SNB-1::GFP fluorescence during the L1 stage. Staged populations of *jsIs37* animals were raised at 22.5°C, then scored at various stages in development for the number of fluorescent patches in the VNC. For each time point, 72 to 114 animals were scored. The average number of patches per animal is plotted as a function of hours after eggs laying (AEL). Developmental stages are shown in bold.

(B and C) Temperature shift analyses. Staged populations of *jsIs37 rpm-1(js317)* animals were raised initially at 15°C (B) or at 22.5°C (C), then shifted once to the corresponding temperature at a particular time in development. Animals were scored as adults for the number of fluorescent patches in the VNC. For each time point, 57 to 131 animals were scored. The average number of patches per animal is plotted as a function of hours after eggs laying (AEL). Developmental stages are shown in bold.

either 15°C or 22.5°C, shifted to the corresponding temperature once during development, then assayed as adults for the average number of fluorescent patches in the VNC. Animals shifted up from the lower permissive to the nonpermissive temperature during embryogenesis or the L1 stage showed few fluorescent patches along the VNC (Figure 4B). In contrast, so long as they remained at the permissive temperature throughout the L1 stage and into part of L2, it did not matter that, subsequently, mutant animals were shifted to the higher nonpermissive temperature. Moreover, even when *rpm-1* mutants were raised at the nonpermissive temperature through embryogenesis, they still showed a greater number of fluorescent patches if shifted to the lower temperature during the first larval stage (Figure 4C). This temporal window of sensitivity, namely, post-embryogenesis through the first larval stage, corresponds to the time when wild-type animals accumulate tagged synaptic vesicles in the VNC (Figure 4A).

rpm-1 Mutations Alter Motor Neuron Cell Morphology and Synaptic Patterning

To determine if mutations in *rpm-1* alter the morphology of other neuronal cell types, we stained with an antibody to synaptotagmin, which marks all synapses (Nonet et al., 1993). *rpm-1* mutant animals do not show any gross changes in neuropil staining patterns. In both wild type and mutant, we observed dense staining along the dorsal nerve cord (DNC), where there is a high concentration of NMJs onto body wall muscle (White et al., 1986) (Figures 5A–5D). *rpm-1* mutants also showed normal organization of VNC and sublateral regions of neuropil (data not shown). Nevertheless, the intensity of anti-synaptotagmin staining was more variable along the DNC (Figures 5C and 5D). To better resolve patterning of synaptic specializations, we stained with an antibody against the *C. elegans* homolog of Rim, a component of the vertebrate active zone (Wang et al., 1997; see Experimental Procedures). In wild type, anti-Rim staining appeared as a dense network of discrete puncta in all neuropil regions, including the DNC (Figures 5E–5H). The total number of puncta in the DNC was variable, even in similarly staged wild-type animals (Table 2). Nevertheless, there were ~25% fewer puncta in the DNC of *rpm-1* mutants. Moreover, anti-Rim puncta were more variably distributed in *rpm-1* animals, forming clusters and gaps typically not seen in wild type (Figures 5E–5H; Table 2). Our analyses do not indicate whether these clusters of labeled presynaptic specializations represent an increased number of active zones in individual neurons or a redistribution of motor neurons, such that those synapses that are present are more closely associated.

We also observed the fluorescence pattern of tagged synaptic vesicles in A-type motor neurons. In the stable strain *jsIs42*, an integrated transgene directs expression of SNB-1::GFP in the three SAB motor neurons, which extend in a straight line toward the nose (Figure 5I). Puncta along these processes correspond to synapses onto head muscle (White et al., 1986). In *rpm-1* mutants, these processes often branch and loop (Figures 5J and 5K), reminiscent of sprouting defects observed in animals with reduced synaptic activity (Zhao and Nonet, 2000). All animals observed showed at least one SAB with abnormal morphology ($n = 71$), and this phenotype was not dependent on temperature. Thus, we show that genetic lesions in *rpm-1* can reduce the number of presynaptic specializations in motor neurons and generate changes in cell morphology suggestive of reduced synaptic activity.

rpm-1 Encodes a Large Conserved Protein

We mapped the *rpm-1* locus between *dpy-11* and *unc-42* on chromosome V, then cloned the gene using positional cloning techniques (Figure 6A). Upon narrowing the locus, we injected cosmids and smaller genomic

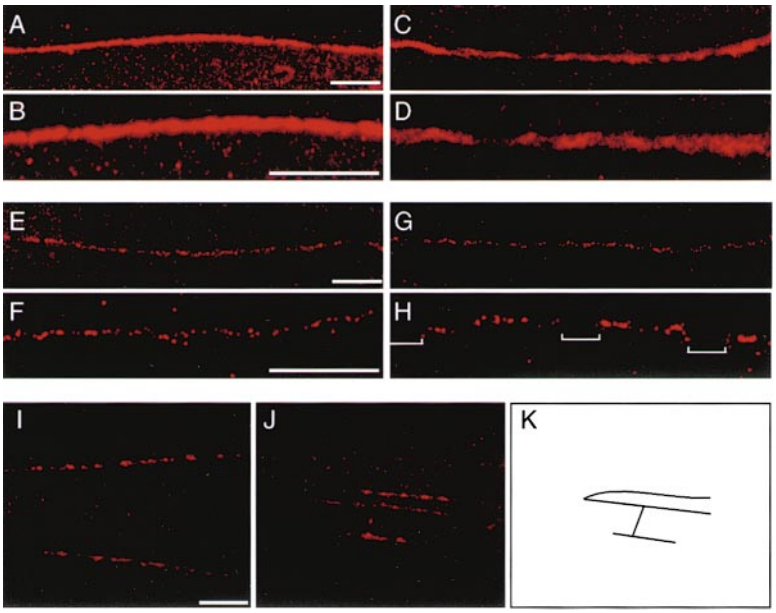

Figure 5. Genetic Lesions in *rpm-1* Alter Synaptic Organization and Morphology of Motor Neurons

(A–J) Confocal images of young adults immunostained with anti-synaptotagmin (A–D and I–J) or anti-Rim (E–H).

(A–D) In *jsIs37* (A) and *jsIs37 rpm-1(js317)* (C), anti-synaptotagmin staining of DNC neuropil shows a similar pattern. Higher magnification of *jsIs37* (B) and *jsIs37 rpm-1(js317)* (D) reveals greater variation in staining intensity.

(E–H) Anti-Rim staining resolves individual puncta and enables quantitation of synaptic patterning in the DNC. Staining of the DNC is similar in *jsIs37* (E) and in *jsIs37 rpm-1(js317)* (G), but higher magnification indicates that puncta in wild type (F) are more densely spaced than in mutant (H). *jsIs37 rpm-1* mutants have fewer puncta in the DNC and more gaps in the staining pattern. Brackets in (H) indicate examples of gaps between puncta in *jsIs37 rpm-1(js317)*.

(I–K) Anti-synaptotagmin staining in SAB motor neurons in the head. Two SAB neurons in wild type reflect the normal simple morphology (I). An SAB neuron in a *jsIs37 rpm-1(js317)* mutant loops and branches (J); (K) schematizes the SAB morphology shown in (J).

Scale bars, 10 μm.

constructs, and assayed for rescue of the GFP phenotype. We found that either of the single cosmids C01B7 or W09B7 contained rescuing activity. The construct pSAM8 (Figure 6B) contains a single predicted open reading frame (ORF), C01B7.6, and is the minimal sequence that rescues the GFP, slight Dpy, and Egl phenotypes. Sequencing of *rpm-1* mutants revealed that the *js410* and *js317* alleles each have a single base pair change that generates a stop codon in the coding sequence (Figure 6C). In sum, we conclude that C01B7.6 encodes the *rpm-1* gene.

The lesions in *js317* and *js410* each generate a stop codon and, therefore, likely complete loss of function for the *rpm-1* gene. Moreover, the GFP pattern in hemizygous animals (i.e., *rpm-1*/Deficiency) phenocopies that of *rpm-1* homozygotes and is no more severe (data not shown). Nevertheless, any interpretation of the null phenotype is confounded by a genomic duplication that we identified in the course of cloning the *rpm-1* gene. In collaboration with the Genome Sequencing Center and the Jin laboratory, we determined that the *C. elegans* genome contains a ~42 kb duplication in tandem (Figure 6A; see Experimental Procedures). This duplication recapitulates a portion of the *rpm-1* ORF (F07B7.X), namely, sequence encoding the N terminal 1951 amino acids, as well as putative regulatory region (Figures 6A–6C). F07B7.X is likely expressed, as it is represented by cDNA. Using oligonucleotides specific to unique sequences at the C terminus of each of these genes (Figure 6C), we confirmed that the *js317* and *js410* lesions indeed are in the *rpm-1* gene, and not in F07B7.X. Although F07B7.X cannot compensate completely for the recessive alleles recovered in our screen, we cannot rule out that RPM-1 and F07B7.X have some functions in common.

We determined the *rpm-1* gene structure based on the sequence of cDNAs mapped to this locus and RT-PCR (see Experimental Procedures). The RPM-1 protein is quite large, containing 3766 amino acids. There is no evidence for alternative splicing. The sequence contains several motifs, including the signature sequence for an RCC1-like domain, two novel repeat sequences ("PHR repeats"), a B-box, and a RING motif. An RCC1 (regulator of chromosome condensation 1) domain contains seven tandem repeats of ~50–60 amino acids (Ohtsubo et al., 1987) and may connote exchange factor activity for a small GTPase (see Discussion). Each PHR (Pam HIW RPM-1) repeat is ~150 amino acids in length; the repeat

Table 2. Altered Presynaptic Patterning in the DNC

Genotype	Total Number of Puncta	Number of Gaps[a] between Puncta	Average Size of Gaps between Puncta	Range of Gap Size	n
jsIs37	895 ± 114.8	4.5 ± 1.4	2.4 μm	1.8–4.3 μm	7 animals
jsIs37 rpm-1 (js317)	685 ± 60.9[b]	12.5 ± 3.7[c]	3.3 μm[d]	1.8–7.5 μm	6 animals

[a] Gaps in the DNC were defined as regions ≥1.8 μm when Rim immunostaining was absent. Gaps <1.8 μm were more prevalent in *rpm-1* mutants than in wild type, but this was not quantified.

[b] $P < 0.005$; different from *jsIs37*.

[c] $P < 0.001$; different from *jsIs37*.

[d] $P < 0.005$; different from *jsIs37*.

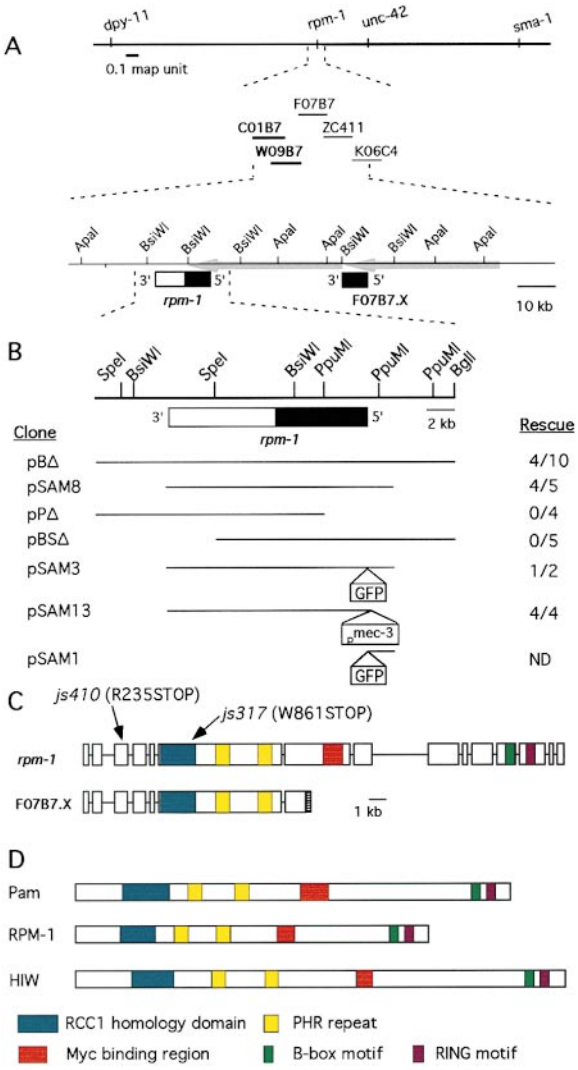

Figure 6. Cloning and Molecular Organization of the *rpm-1* Gene

(A) *rpm-1* maps to chromosome V, between *dpy-11* and *unc-42* on the genetic map. The cosmids C01B7 and W09B7 (bold) each contain rescuing activity for the GFP, slight Dpy, and Egl phenotypes of *rpm-1* mutants. Transformation rescue with smaller genomic fragments (see [B]) indicates that the predicted ORF C01B7.6 encodes the *rpm-1* gene (partially closed box). A 42 kb duplication in tandem, as indicated by the gray arrows, includes part of the *rpm-1* coding sequence (F07B7.X, closed box). The similar orientation of *rpm-1* and F07B7.X is indicated by 5′ and 3′ designations. Select restriction enzymes are shown.

(B) Genomic constructs used to confirm identity and determine expression of the *rpm-1* gene. The *rpm-1* ORF is indicated (box and restriction map from [A] are magnified). Lines indicate the extent of each genomic clone. Each clone was injected into *jsIs37 rpm-1(js317)*, and germline transformants were assayed for the presence of tagged vesicle fluorescence in the VNC. For each construct, the number of transformant lines that rescued out of the total assayed is shown. We confirmed that pSAM8 also rescued the GFP, Dpy, and Egl phenotypes in *jsIs37 rpm-1(js410)* (2 of 3 lines).

(C) The exon (boxes) and intron (lines) structure of *rpm-1* and F07B7.X. Color coding of predicted protein motifs is the same in (C) and (D) (see key, [D]). The position of the genetic lesion in each of the two *rpm-1* alleles is shown. The horizontal hatched box at the F07B7.X C terminus represents coding sequence unique to the F07B7.X predicted ORF.

(D) Conserved arrangement of protein motifs in RPM-1 and homologs. Motifs for each of the proteins hPam (4641 aa), *C. elegans* RPM-1 (3766 aa), and *Drosophila* HIW (5233 aa) are color coded. The Myc binding domain was defined in Guo et al. (1998). PHR repeat sequence was first identified by Guo et al. (1998) but was extended to 150 amino acid domains based on BLAST alignment. Other predictions are based on SMART (Schultz et al., 1998) and BLAST (Altschul et al., 1997). As aligned by BLAST, the overall identity between RPM-1 and hPam is 31%; the overall identity between RPM-1 and HIW is 32%.

sequence does not provide clues as to function. B-box and RING motifs are cysteine rich regions that bind to zinc and mediate protein–protein interactions (reviewed by Borden, 1998).

A BLAST search indicates that RPM-1 has significant homology to the human protein Pam (hPam) (Figure 6D), named for its association with the protooncogene Myc (Guo et al., 1998). There is homology across the entire ORF (31%), with greatest conservation at the C terminus (57% identity over ~280 amino acids). Significantly, highest levels of hPam expression are in brain and thymus, though the gene appears to be expressed in several tissue types. Immunostaining of human aortic endothelial cells indicates that hPam sometimes is nuclearly localized, consistent with its affinity for Myc. Nevertheless, RPM-1 and hPam may have some distinct functions. Alignment of the two protein sequences suggests that RPM-1 is missing 168 of the 301 amino acids in Pam that bound to Myc (Figure 6C). Further, our analyses of RPM-1 expression indicate that this protein is not restricted to the nucleus (see below). Finally, the completed genome sequence of *C. elegans* has not revealed a Myc homolog (*C. elegans* Sequencing Consortium, 1998; Yuan et al., 1998). *rpm-1* also is represented in the *Drosophila* genome, by the ortholog *highwire* (Wan et al., 2000). The gene product HIW is larger than RPM-1 or hPam (Figure 6D) but, like its orthologs, is neuronally expressed. Subcellularly, HIW is localized to presynaptic terminals at the NMJ; loss-of-function mutations generate an increase in the number of boutons (Wan et al., 2000).

rpm-1 Is Expressed in Neurons

To determine those cell types that express the *rpm-1* gene, we designed a promoter fusion DNA construct (pSAM1), attaching GFP to ~2 kb of putative native promoter sequence (Figure 6B). Wild-type animals transformed with this construct show GFP fluorescence in most, if not all, neurons (Figure 7A). Fluorescence first appears in comma stage embryos and persists through adulthood. In addition to neurons, we observe expression in the pharynx, in coelomocytes, and in the distal tip cell, a somatic gonad cell type that often displays neuronal characteristics (data not shown). Notably, expression of this promoter construct suggests that *rpm-1* is not expressed in body wall muscle, hypodermis, or intestine. To visualize subcellular RPM-1 localization, we transformed with the construct pSAM3, which fuses GFP in-frame with the full-length coding sequence (Figure 6B). The GFP signal in pSAM3 transformants is weak, enabling us to visualize that expression of this full-length RPM-1 construct can rescue the SNB-1::GFP pattern in *rpm-1* mutants (data not shown). Expression of the pSAM3 rescuing construct indicates that RPM-1 is most

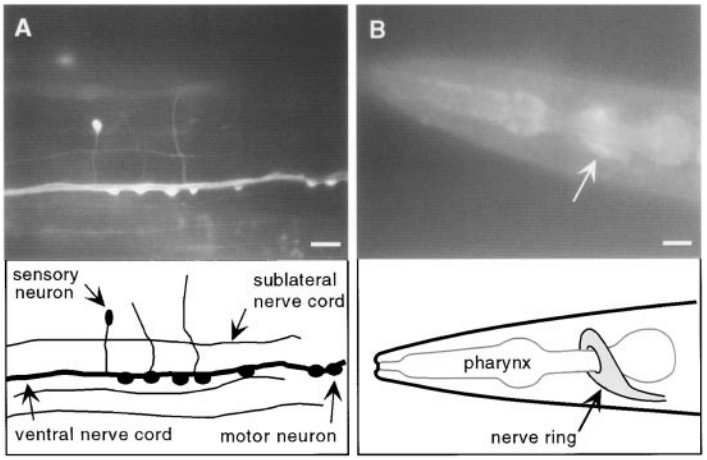

Figure 7. *rpm-1* Neuronal Expression

(A) Epifluorescence image of a single focal plane and schematic showing cell types that express GFP driven by the *rpm-1* promoter (pSAM1; see Figure 6). Fluorescence is visible in a mechanosensory neuron, several motor neurons, and VNC and sublateral neuropil regions.

(B) GFP expression in an *rpm-1(js317)* mutant transformed with full-length RPM-1 tagged with GFP (pSAM3; see Figure 6), and schematic of the *C. elegans* head. The pSAM3 genomic construct rescues the *rpm-1(js317)* phenotypes and is predicted to reflect subcellular localization of RPM-1. GFP fluorescence is not restricted to nuclei, as it is present in the nerve ring neuropil (arrow), which envelops the pharynx.

Scale bars, 10 μm.

abundant in axons of the nerve ring neuropil (Figure 7B). Clearly, RPM-1 is not confined to the nucleus.

RPM-1 Functions Cell Autonomously

To determine if RPM-1 functions in mechanosensory neurons, we generated mosaic animals in an *rpm-1* mutant background. Using the *mec-3* promoter (Way and Chalfie, 1989), we directed expression of the wild-type *rpm-1* gene in the mechanosensory neurons and two other neuronal cell types (pSAM13) (Figure 6). In pSAM13 transformants, the wild-type pattern of tagged vesicle fluorescence in the VNC is restored (Figure 8). Likewise, the phenotype of ectopic axonal targeting is rescued (data not shown). Expression restricted to the presynaptic mechanosensory neurons does not rescue the slight Dpy or Egl phenotype. Thus, RPM-1 can function cell autonomously in the presynaptic mechanosensory neurons to regulate localization of synaptic vesicles and to ensure the wild-type cell morphology.

Discussion

rpm-1 Mutations Alter Targeting and Synaptogenesis

We have exploited the simple morphology and defined circuitry of the mechanosensory neurons to study molecular mechanisms of synaptogenesis. Our screen for disruptions of presynaptic patterning in mechanosensory neurons uncovered *rpm-1*. Lesions in *rpm-1* disrupt the stereotypic pattern of tagged vesicle fluorescence that we observe in wild-type mechanosensory neurons: fluorescent patches are absent from the VNC, and there are fewer puncta in the nerve ring. Those PLM synaptic branches that target to the VNC are unstable and retract later in development. In addition, we observe that the PLM axon aberrantly targets to the VNC in *rpm-1* mutants. Unlike the synaptic branch, this ectopic extension is stable and not subject to changes in temperature. It is unclear if, in *rpm-1* mutants, synapses form where the PLM axon ectopically enters the VNC. The neurons that ordinarily are postsynaptic at the PLM en passant synapses extend axons along the length of the VNC, so are present where the PLM axon aberrantly enters and fasciculates with the VNC axon bundle. At the light level, we clearly do not observe inappropriately placed accumulations of SNB-1::GFP fluorescence. It is possible, however, that widely spaced synapses form and are not detectable by our tagged vesicle marker.

Loss of RPM-1 function alters motor neuron morphology. The cholinergic SAB motor neurons, which innervate head muscle, normally show a linear morphology. In *rpm-1* mutants, these axons overgrow, loop, and branch. In the DNC, which contains inhibitory GABAergic and excitatory cholinergic synapses, *rpm-1* mutants show fewer presynaptic specializations, and organization of these synapses is altered. Zhen et al. (2000) independently observed these changes in the DNC of

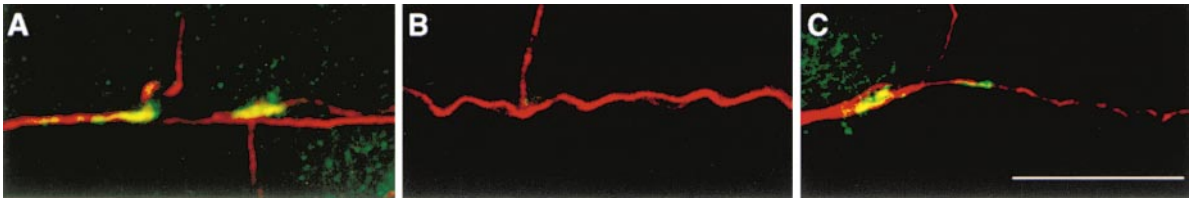

Figure 8. Presynaptic Expression of RPM-1 Rescues Synaptogenesis Defect

Confocal images of young adult animals, showing immunostaining of anti-GFP (green) and anti-MEC-7 (red), which labels mechanosensory neurons.

(A) Anti-GFP immunostaining shows the wild-type pattern of two fluorescent patches in the VNC, corresponding to accumulations of tagged synaptic vesicle fluorescence in each of the bilateral PLM neurons.

(B) GFP-tagged vesicles are absent in the VNC of *rpm-1(js317)*.

(C) Expression of RPM-1 in mechanosensory neurons, under control of the *mec-3* promoter, restores the wild-type pattern of tagged vesicle fluorescence. Scale bar, 10 μm.

rpm-1 mutants upon screening for disruption of SNB-1::GFP patterning in GABAergic motor neurons.

Certain phenotypes in *rpm-1* mutants, including the failure to accumulate tagged vesicle fluorescence along the VNC, are temperature sensitive. The results of our temperature shift experiments demonstrate that there is a discrete window of sensitivity and that this window coincides with synaptic vesicle accumulation at PLM synapses in normal development. Our molecular and genetic data suggest that the two *rpm-1* alleles we isolated represent complete loss-of-function mutations. Both alleles are recessive and phenotypically similar. The *js317* allele, in *trans* to a deficiency that deletes this genomic region, is viable and shows the same patterning of GFP fluorescence observed in *js317* homozygotes. The *js317* and *js410* lesions are early stop codons, so are predicted to severely truncate the protein. These data suggest that RPM-1 protein is absent in the mutants. Accordingly, our shift experiments comment on mechanism rather than protein function and reveal a mechanism that is temperature sensitive in the absence of RPM-1. We note, however, that interpretation of the shift data is complicated by the gene F07B7.X, encoding a duplication of the first 1950 amino acids of RPM-1. F07B7.X is likely expressed and retains the RCC1 and PHR motifs found in RPM-1. Thus, the F07B7.X gene product may share certain functions in common with RPM-1. If this is so, our shift data would reflect manipulation of this "RPM-1" activity.

Regardless of any possible RPM-1 function in the mutants, (1) there is a particular time, namely, early larval development, when *rpm-1* mutants are temperature sensitive, and (2) during this time, the requirement for RPM-1 can be bypassed via maintenance at a lower temperature. The simplest explanation for these data is that RPM-1 function ordinarily is required during the period of synaptogenesis.

What Is RPM-1's Role in Neuronal and Synaptic Development?

We demonstrate that RPM-1 functions cell autonomously to regulate neuronal morphology. What mechanism in the presynaptic mechanosensory neurons is regulated in vivo by RPM-1? There are at least two possibilities. First, RPM-1 could regulate neuronal maturation. Our data are consistent with a model whereby mechanosensory synapses fail to mature, generating retraction of the synaptic branch. Although we observe fewer synaptic branches than in wild type, additional transient branches could be missed in our analyses of staged populations. Such growth cone dynamics would be consistent with the 20–55 μm/hr pace of VD motor neuron migration observed by Knobel et al. (1999). Moreover, if RPM-1 is a regulator of synaptic maturation, the *rpm-1* mutant phenotype of ectopic axonal targeting could be secondary to failure to form stable synapses. Perhaps such failure generates a retrograde signal, which leads to ectopic growth toward the VNC. Alternatively, the ectopic growth could be a primary defect, resulting from failure of the axonal growth cone to mature into a stable and static structure in the lateral midbody region.

In a different scenario, RPM-1 could be involved in mechanisms of outgrowth at the appropriate subcellular locus. Normally, PLM extends a synaptic branch perpendicularly from the middle of the axon, in a defined region between PVM and the vulva. Perhaps, in *rpm-1* mutants, the machinery for synaptic branch extension is misrouted to the inappropriate intracellular location (Schuman, 1999). On the other hand, such machinery could normally be distributed uniformly along the axon, but local cues regulating the locus of branch extension are somehow disrupted in *rpm-1* animals. We note that normal and ectopic targeting are not mutually exclusive: a single PLM neuron can display both a synaptic branch and ectopic growth from the end of the axon.

We favor the first hypothesis, that RPM-1 is part of a mechanism to effect neuronal maturation. This explanation is more consistent with the phenotype of synaptic branch retraction. Moreover, a role in maturation is compatible with the motor neuron phenotypes. We observed that the SAB motor neurons in *rpm-1* sprouted additional branches, similar to sprouting in SAB neurons induced by deficits in synaptic activity (Zhao and Nonet, 2000). In the DNC neuropil, there were fewer presynaptic densities (see also Zhen et al., 2000). Wider gaps between these labeled presynaptic specializations could simply reflect that many specializations are missing in mutant animals. We also observed that labeled presynaptic specializations in the DNC appeared to aggregate. Perhaps these aggregations represent the addition of active zones within individual motor neurons. Alternatively, they may be generated by a redistribution of existing synapses.

Our observations of these changes in presynaptic labeling and in morphology of mechanosensory and motor neurons thus may reflect a primary defect in synapse formation. Failure of synapses to form or to mature may, in turn, generate distinct cellular responses, depending on cell type. Such diverse effects would be consistent with prior demonstrations in *C. elegans* of differential sensitivity to perturbations in activity (Peckol et al., 1999; Zhao and Nonet, 2000). In this regard, we note that lesions in the *Drosophila* ortholog HIW generate a reduction in quantal content at the *Drosophila* NMJ and an increase in the number of branches and boutons (Wan et al., 2000).

If indeed RPM-1 is involved in neuronal maturation at the time of synaptogenesis, its function is not absolutely required: labeling with synaptic markers indicates that many synapses do differentiate in *rpm-1* animals. Neuronal patterning is grossly normal. For our screen, we did not predict a gross behavioral phenotype from loss, per se, of chemical synapses made by mechanosensory neurons; these synapses are not required for the touch response (Chalfie et al., 1985). Nevertheless, the essentially normal behavior of mutant animals confirms that there are no general synaptic defects.

How Does RPM-1 Function?

The RPM-1 protein is huge, containing 3766 amino acids. There are several predicted motifs, including a B-box, RING finger, and RCC1 domain and two repeats of unknown function. B-box and RING domains are cysteine rich motifs that bind to zinc and mediate protein–protein interactions; they are found in numerous proteins with diverse functions (reviewed by Saurin et al.,

1996; Borden, 1998). Thus, RPM-1 may bind to or anchor other proteins at the appropriate subcellular location. The RCC1 motif may provide a clue about activity; however, functional information about RCC1 domains is limited. RCC1 domains comprise repeats of 50–60 amino acids (Ohtsubo et al., 1987). A crystal structure of these repeats predicts a seven-bladed propeller, similar to that of WD40 repeats (Renault et al., 1998). The human RCC1 protein was the first described (Ohtsubo et al., 1987). It was cloned based on ability to rescue a premature chromosome condensation phenotype in a hamster cell line (Nishimoto et al., 1978, 1981). This original RCC1 protein acts as an exchange factor for the small GTPase Ran and functions in import and export from the nucleus (Bischoff and Ponstingl, 1991). Several additional RCC1-containing proteins have been identified in eukaryotes (Meindl et al., 1996; Lehman et al., 1998; Uhlmann et al., 1999). While functions have not been described for many of these proteins, it has been shown that each of the two RCC1 domains in the HERC1 protein has distinct biochemical activities, namely, interaction with clathrin and exchange factor activity for the small GTPases ARF1, Rab3A, and Rab5 (Rosa et al., 1996; Rosa and Barbacid, 1997).

Perhaps RPM-1 acts as an exchange factor for a small GTPase. This function would be consistent with the defined role of small GTPases in neuronal morphology (reviewed by Hall, 1998). For example, constitutively active Rac1 in mouse Purkinje cells caused a reduction in the number of axon terminals but generated more numerous, smaller dendritic spines that often had more than one synapse (Luo et al., 1996). In *Drosophila*, the exchange factor encoded by the *still life* gene is found at the presynaptic nerve terminal (Sone et al., 1997). Expression of a truncated protein generated a range of targeting and maturation defects, including axons that failed to form terminal arbors and terminal arbors that did form but contained shorter processes and fewer boutons.

C. elegans RPM-1 shares homology with hPam (Guo et al., 1998). There is conservation across the entire ORF, with greatest identity at the C terminus, where each encodes zinc binding motifs. hPam expression is highest in brain and thymus. Expression in human cell lines indicates that it is present in the nucleus. Nevertheless, no function has been described for hPam. Moreover, the significance of this homology is unclear. Although Pam was cloned based on its association with Myc, sequencing of the *C. elegans* genome has not disclosed a Myc homolog (*C. elegans* Sequencing Consortium, 1998; Yuan et al., 1998). Further, there is a deletion in RPM-1 in the region corresponding to the Myc binding domain.

Our data for localization of GFP generated by a rescuing DNA construct indicate that the RPM-1 protein is cytoplasmic and most abundant in regions highly populated with synapses. Zhen et al. (2000) show by immunostaining that RPM is at synapses. Similarly, the *Drosophila* protein is synaptically localized (Wan et al., 2000). In sum, RPM-1 appears to be acting at the synapse in diverse neuronal cell types and can act cell autonomously to regulate accumulation of synaptic vesicles and stabilization of mature neuronal morphology. It remains to be determined whether hPam may have a similar role at vertebrate synapses.

Experimental Procedures

Strains and Genetics

Strains were grown at 22.5°C, unless otherwise specified, and were maintained as described by Sulston and Hodgkin (1988). The non-complementing *rpm-1* alleles *js317* and *js410* were isolated in a clonal screen for changes in the pattern of SNB-1::GFP fluorescence in the mechanosensory neurons (Nonet, 1999). Specifically, following mutagenesis with ethylmethane sulfonate, F1 animals were placed on individual plates and allowed to self-fertilize. For screening, 15–20 F1 L4s or young adults from each F1 plate were mounted on a 2% agar pad containing 2 μl of 10 mM NaN_3 and analyzed under epifluorescence for the pattern of SNB-1::GFP fluorescence. In this way, we screened 2032 haploid genomes. Strains showing a phenotype of interest were confirmed to be heritable, and mutants were backcrossed to N2 four times. We confirmed that GFP in *rpm-1* mutants continues to tag synaptic vesicles, by observing that GFP fluorescence mislocalizes to the soma when the kinesin UNC-104 (Hall and Hedgecock, 1991) is disrupted.

Microscopy

Most observations were made under epifluorescence using an Olympus B-MAX 60 with 60× and 100× objectives. Images from the compound microscope were acquired using a Dage SIT68 linked to a CG-7 frame grabber using NIH Image software (Scion). Confocal images were acquired on an Olympus Fluoview confocal microscope.

Temperature Shift Experiments and Developmental Analyses

Animals were staged by allowing 80–100 adult hermaphrodites to lay eggs on an agar plate for 1 hr, then transferring the adults. For the shift experiments, staged animals were raised either at 15°C or at 22.5°C for various lengths of time during development, then shifted to the higher or lower temperature. Adult animals were scored for the number of GFP fluorescence accumulations along the VNC. For developmental analyses, animals were scored at designated hours after egg laying. Scoring required mounting animals on a 2% agar pad containing 10 mM NaN_3, then viewing under epifluorescence.

Cloning and Molecular Characterization of *rpm-1*

rpm-1 was cloned using a positional cloning strategy. Genetic mapping was performed in a *jsIs37* genetic background to permit visualization of the PLM synaptic varicosities. *rpm-1(js317)* was mapped to the *dpy-11 unc-42* interval by Tc1 mapping (Williams et al., 1992). From *rpm-1(js317)/dpy-11(e224) unc-42(e270)* heterozygotes, 13 of 16 Dpy non-Unc recombinants and 3 of 14 Unc non-Dpy recombinants carried the *rpm-1* lesion. To further refine the physical position of *rpm-1*, deficiencies in the region were tested for their ability to complement the GFP phenotype; *mDf1*, *sDf47*, and *sDf29* failed to complement, while *nDf31* complemented *rpm-1*. Overlapping cosmids that spanned the interval between the left breakpoint of *mDf1* and the right breakpoint of *sDf47* were injected into mutant animals, and germline transformants were assayed for the presence of fluorescent patches in the VNC. Cosmids initially were injected in pools; cosmids in the rescuing pool were then injected individually. The cosmids C01B7 (GenBank accession number U53147) and W09B7 (GenBank accession number AC006697) each were able to rescue the *rpm-1* GFP phenotype, indicating rescuing activity in the region of cosmid overlap. A series of subclones that subdivided the overlap interval was constructed and tested for rescuing activity. A subclone containing the complete Genefinder-predicted ORF C01B7.6 (GenBank accession number AAA96117) contained rescuing activity. Clones containing the flanking-predicted ORFs and clones deleting the C- or N-terminal regions of C01B7.6 all failed to rescue.

A composite cDNA sequence was assembled for *rpm-1* from cDNA EST clones yk34a10, yk397f1, and yk61d6 and from specific cDNA fragments amplified from first strand cDNA by RT-PCR using the predicted ORF as a guide. An SL1 *trans*-spliced leader was

present 71 bp upstream of the ATG of C01B7.6 in cDNA amplified by RT-PCR. The full-length *rpm-1* cDNA we assembled was identical to the predicted gene C01B7.6. The *js317* and *js410* lesions were identified by sequencing PCR products representing the entire coding sequence and all exon–intron boundaries. All sequencing was performed on an ABI sequencer.

Duplication of *rpm-1* Coding Sequences

Southern analyses and sequencing of genomic DNA in the *rpm-1* mutants and the EST cDNA yk238a6 provided evidence for a genomic duplication. The Genome Sequencing Center (Washington University School of Medicine) provided sequence of the cosmid clone F07B7 (GenBank accession number AC024696), which contains the duplication breakpoint. Identification of the duplication requires revision of the physical map, as previously described; this genomic region is represented by clones (from left to right) C01B7, W09B7, F07B7, EGAP798 (GenBank accession number AC027664), and ZC411 (GenBank accession number U53146).

Analysis of F07B7 sequence indicates that the duplicated region consists of 42,095 bp, which includes the *rpm-1* promoter and first 1,951 amino acids of *rpm-1* coding region. The relative intensity of bands visualized by Southern blot using probes adjacent to the duplication breakpoint indicates that the sequences encoding *rpm-1* and F07B7.X are present in similar copy number. The duplication is present in all the Bristol background strains we analyzed and is absent from wild-type isolates RC301, CB4856, and CB4855, as assayed by PCR for the duplication breakpoint.

Plasmid Constructions

pB and pP were constructed from cosmid W09B7 by digestion with BglI and PpuMI, respectively, and unimolecular religation. pBS was constructed from pB by digestion with SpeI followed by religation. pSAM1, a promoter fusion that fuses GFP at the initiation codon, was constructed by ligation of a 2.1 kb PCR product digested with SphI and NgoMI into pPD117.01 cut with SphI and AgeI. The full-length GFP::RPM-1 plasmid pSAM3 was constructed starting with pSAM1. First, an 800 bp fragment containing engineered EcoRI and SacII sites upstream of the RPM-1 ATG codon and an engineered NheI restriction site in the second intron was amplified from genomic DNA, digested with EcoRI and NheI, and inserted into EcoRI-NheI-digested pSAM1 to create pSAM2. pSAM2 was digested with AgeI and NheI, and a 2.7 kb AgeI-NheI genomic fragment was ligated in to create pSAM2D. pSAM2D was digested with NheI and StuI; an 11.75 kb NheI-SnaBI genomic fragment from the pB clone was inserted to create pSAM3. pSAM8 was created by deleting the GFP cassette from pSAM3. To construct pSAM13, the *rpm-1* promoter of pSAM8 was replaced by a 2.0 kb SacII-PstI *mec-3* promoter fragment from pPD56.57.

Germline Transformation

DNA was prepared for injection using the Qiagen kit. Plasmids (10–20 μg/ml) and cosmids (10 μg/ml) were injected using the standard methods (Mello and Fire, 1995), using *rol-6* DNA pRF4 (140 μg/ml) as a transformation marker.

Immunocytochemistry

Animals were fixed using Bouin's fixative for whole-mount immunocytochemistry and stained with antibodies directed against synaptotagmin (Nonet et al., 1993), syntaxin (Saifee et al., 1998), SNB-1 (Nonet et al., 1998), GFP (mouse monoclonal, Clonetech), MEC-7 (Mitani et al., 1993), or *C. elegans* Rim as previously described (Saifee et al., 1998). *C. elegans* Rim (GenBank accession number AF257062) is encoded by the *unc-10* gene (G. D. H. et al., unpublished data; Wang et al., 1997). The polyclonal antibody against Rim was generated by immunizing rabbits with a bacterial product representing amino acids 1–142 fused to a his_6 tag. Specificity of the antibody was confirmed by lack of immunoreactivity in an *unc-10(md1117)* mutant, in which the entire Rim coding region is deleted.

Acknowledgments

We thank the Jin laboratory and Goodman laboratory for sharing unpublished observations; the Jin laboratory, Pat Mink, John Spieth, and the Genome Sequencing Center for sharing data regarding the duplication of *rpm-1* sequences; members of the Nonet laboratory for comments on the manuscript; Poupak Rahmani and Don Moerman for sharing deficiency breakpoint data; Yuji Kohara for EST cDNAs; Guoqiang Gu, Miriam Goodman, and Marty Chalfie for the *uIs25* strain and anti-MEC-7 antibodies; and Andy Fire for GFP vectors. Some strains used in this work were obtained from the Caenorhabditis Genetics Center. A. M. S. was supported by National Institutes of Health predoctoral training grant GM07067. This work was funded by grants to M. L. N. from the Searle Scholar Program and the McKnight Foundation for Neuroscience.

Received April 24, 2000; revised April 27, 2000.

References

Altschul, S.F., Madden, T.L., Schaffer, A.A., Zhang, J., Zhang, Z., Miller, W., and Lipman, D.J. (1997). Gapped BLAST and PSI-BLAST: a new generation of protein database search programs. Nucleic Acids Res *25*, 3389–3402.

Bischoff, F.R., and Ponstingl, H. (1991). Catalysis of guanine nucleotide exchange on Ran by the mitotic regulator RCC1. Nature *354*, 80–82.

Borden, K.L. (1998). RING fingers and B-boxes: zinc-binding protein–protein interaction domains. Biochem. Cell Biol. *76*, 351–358.

Burgess, R.W., Nguyen, Q.T., Son, Y.J., Lichtman, J.W., and Sanes, J.R. (1999). Alternatively spliced isoforms of nerve- and muscle-derived agrin: their roles at the neuromuscular junction. Neuron *23*, 33–44.

C. elegans Sequencing Consortium (1998). Genome sequence of the nematode *C. elegans*: a platform for investigating biology. Science *282*, 2012–2018.

Chalfie, M., and Au, M. (1989). Genetic control of differentiation of the *Caenorhabditis elegans* touch receptor neurons. Science *243*, 1027–1033.

Chalfie, M., Sulston, J.E., White, J.G., Southgate, E., Thomson, J.N., and Brenner, S. (1985). The neural circuit for touch sensitivity in *Caenorhabditis elegans*. J. Neurosci. *5*, 956–964.

Chalfie, M., Tu, Y., Euskirchen, G., Ward, W.W., and Prasher, D.C. (1994). Green fluorescent protein as a marker for gene expression. Science *263*, 802–805.

Craig, A.M. (1998). Activity and synaptic receptor targeting: the long view. Neuron *21*, 459–462.

Dai, Z., and Peng, H.B. (1995). Presynaptic differentiation induced in cultured neurons by local application of basic fibroblast growth factor. J. Neurosci. *15*, 5466–5475.

Dai, Z., and Peng, B. (1996). From neurite to nerve terminal: induction of presynaptic differentiation by target-derived signals. Semin. Neurosci. *8*, 97–106.

Emmons, S.W., and Sternberg, P.W. (1997). Male development and mating behavior. In *C. elegans* II, D.L. Riddle et al., eds. (Cold Spring Harbor, NY: Cold Spring Harbor Laboratory Press), pp. 295–334.

Garrity, P.A., and Zipursky, S.L. (1995). Neuronal target recognition. Cell *83*, 177–185.

Guo, Q., Xie, J., Dang, C.V., Liu, E.T., and Bishop, J.M. (1998). Identification of a large Myc-binding protein that contains RCC1-like repeats. Proc. Natl. Acad. Sci. USA *95*, 9172–9177.

Hall, A. (1998). Rho GTPases and the actin cytoskeleton. Science *279*, 509–514.

Hall, D.H., and Hedgecock, E.M. (1991). Kinesin-related gene *unc-104* is required for axonal transport of synaptic vesicles in C. elegans. Cell *65*, 837–847.

Hall, Z.W., and Sanes, J.R. (1993). Synaptic structure and development: the neuromuscular junction. Cell *72 (Suppl.)*, 99–121.

Hamelin, M., Scott, I.M., Way, J.C., and Culotti, J.G. (1992). The *mec-7* beta-tubulin gene of *Caenorhabditis elegans* is expressed primarily in the touch receptor neurons. EMBO J. *11*, 2885–2893.

Hart, A.C., Sims, S., and Kaplan, J.M. (1995). Synaptic code for

sensory modalities revealed by *C. elegans* GLR-1 glutamate receptor. Nature *378*, 82–85.

Knobel, K.M., Jorgensen, E.M., and Bastiani, M.J. (1999). Growth cones stall and collapse during axon outgrowth in *Caenorhabditis elegans*. Development *126*, 4489–4498.

Lehman, A.L., Nakatsu, Y., Ching, A., Bronson, R.T., Oakey, R.J., Keiper-Hrynko, N., Finger, J.N., Durham-Pierre, D., Horton, D.B., Newton, J.M., et al. (1998). A very large protein with diverse functional motifs is deficient in rjs (runty, jerky, sterile) mice. Proc. Natl. Acad. Sci. USA *95*, 9436–9441.

Luo, L., Hensch, T.K., Ackerman, L., Barbel, S., Jan, L.Y., and Jan, Y.N. (1996). Differential effects of the Rac GTPase on Purkinje cell axons and dendritic trunks and spines. Nature *379*, 837–840.

Maricq, A.V., Peckol, E., Driscoll, M., and Bargmann, C.I. (1995). Mechanosensory signaling in *C. elegans* mediated by the GLR-1 glutamate receptor. Nature *378*, 78–81.

Meindl, A., Dry, K., Herrmann, K., Manson, F., Ciccodicola, A., Edgar, A., Carvalho, M.R., Achatz, H., Hellebrand, H., Lennon, A., et al. (1996). A gene (RPGR) with homology to the RCC1 guanine nucleotide exchange factor is mutated in X-linked retinitis pigmentosa (RP3). Nat. Genet. *13*, 35–42.

Mello, C., and Fire, A. (1995). DNA transformation. In *Caenorhabditis elegans*: Modern Analysis of an Organism, H.F. Epstein and D.C. Shakes, eds. (San Diego: Academic Press), pp. 451–482.

Mitani, S., Du, H., Hall, D.H., Driscoll, M., and Chalfie, M. (1993). Combinatorial control of touch receptor neuron expression in *Caenorhabditis elegans*. Development *119*, 773–783.

Nishimoto, T., Eilen, E., and Basilico, C. (1978). Premature of chromosome condensation in a *ts* DNA-mutant of BHK cells. Cell *15*, 475–483.

Nishimoto, T., Ishida, R., Ajiro, K., Yamamoto, S., and Takahashi, T. (1981). The synthesis of protein(s) for chromosome condensation may be regulated by a post-transcriptional mechanism. J. Cell Physiol. *109*, 299–308.

Noakes, P.G., Gautam, M., Mudd, J., Sanes, J.R., and Merlie, J.P. (1995). Aberrant differentiation of neuromuscular junctions in mice lacking s-laminin/laminin beta 2. Nature *374*, 258–262.

Nonet, M.L. (1999). Visualization of synaptic specializations in live *C. elegans* with synaptic vesicle protein–GFP fusions. J. Neurosci. Methods *89*, 33–40.

Nonet, M.L., Grundahl, K., Meyer, B.J., and Rand, J.B. (1993). Synaptic function is impaired but not eliminated in *C. elegans* mutants lacking synaptotagmin. Cell *73*, 1291–1305.

Nonet, M.L., Saifee, O., Zhao, H., Rand, J.B., and Wei, L. (1998). Synaptic transmission deficits in *Caenorhabditis elegans* synaptobrevin mutants. J. Neurosci. *18*, 70–80.

Ohtsubo, M., Kai, R., Furuno, N., Sekiguchi, T., Sekiguchi, M., Hayashida, H., Kuma, K., Miyata, T., Fukushige, S., Murotsu, T., et al. (1987). Isolation and characterization of the active cDNA of the human cell cycle gene (RCC1) involved in the regulation of onset of chromosome condensation. Genes Dev. *1*, 585–593.

Peckol, E.L., Zallen, J.A., Yarrow, J.C., and Bargmann, C.I. (1999). Sensory activity affects sensory axon development in *C. elegans*. Development *126*, 1891–1902.

Renault, L., Nassar, N., Vetter, I., Becker, J., Klebe, C., Roth, M., and Wittinghofer, A. (1998). The 1.7 Å crystal structure of the regulator of chromosome condensation (RCC1) reveals a seven-bladed propeller. Nature *392*, 97–101.

Rosa, J.L., and Barbacid, M. (1997). A giant protein that stimulates guanine nucleotide exchange on ARF1 and Rab proteins forms a cytosolic ternary complex with clathrin and Hsp70. Oncogene *15*, 1–6.

Rosa, J.L., Casaroli-Marano, R.P., Buckler, A.J., Vilaro, S., and Barbacid, M. (1996). p619, a giant protein related to the chromosome condensation regulator RCC1, stimulates guanine nucleotide exchange on ARF1 and Rab proteins. EMBO J. *15*, 4262–4273.

Saifee, O., Wei, L., and Nonet, M.L. (1998). The *Caenorhabditis elegans unc-64* locus encodes a syntaxin that interacts genetically with synaptobrevin. Mol. Biol. Cell *9*, 1235–1252.

Sanes, J.R. (1997). Genetic analysis of postsynaptic differentiation at the vertebrate neuromuscular junction. Curr. Opin. Neurobiol. *7*, 93–100.

Sanes, J.R., and Lichtman, J.W. (1999). Development of the vertebrate neuromuscular junction. Annu. Rev. Neurosci. *22*, 389–442.

Saurin, A.J., Borden, K.L., Boddy, M.N., and Freemont, P.S. (1996). Does this have a familiar RING? Trends Biochem. Sci. *21*, 208–214.

Schultz, J., Milpetz, F., Bork, P., and Ponting, C.P. (1998). SMART, a simple modular architecture research tool: identification of signaling domains. Proc. Natl. Acad. Sci. USA *95*, 5857–5864.

Schuman, E.M. (1999). mRNA trafficking and local protein synthesis at the synapse. Neuron *23*, 645–648.

Son, Y.J., Patton, B.L., and Sanes, J.R. (1999). Induction of presynaptic differentiation in cultured neurons by extracellular matrix components. Eur. J. Neurosci. *11*, 3457–3467.

Sone, M., Hoshino, M., Suzuki, E., Kuroda, S., Kaibuchi, K., Nakagoshi, H., Saigo, K., Nabeshima, Y., and Hama, C. (1997). Still life, a protein in synaptic terminals of *Drosophila* homologous to GDP–GTP exchangers. Science *275*, 543–547.

Sulston, J., and Hodgkin, J. (1988). Methods. In The Nematode *Caenorhabditis elegans*, W.B. Wood, ed. (Cold Spring Harbor, NY: Cold Spring Harbor Laboratory Press), pp. 587–606.

Sulston, J.E., and Horvitz, H.R. (1977). Post-embryonic cell lineages of the nematode, *Caenorhabditis elegans*. Dev. Biol. *56*, 110–156.

Sulston, J.E., Schierenberg, E., White, J.G., and Thomson, J.N. (1983). The embryonic cell lineage of the nematode *Caenorhabditis elegans*. Dev. Biol. *100*, 64–119.

Uhlmann, J., Wiemann, S., and Ponstingl, H. (1999). DelGEF, an RCC1-related protein encoded by a gene on chromosome 11p14 critical for two forms of hereditary deafness. FEBS Lett. *460*, 153–160.

Wan, H.I., DiAntonio, A., Fetter, R.D., Bergstrom, K., Strauss, R., and Goodman, C.S. (2000). Highwire regulates synaptic growth in *Drosophila*. Neuron *26*, this issue, 313–329.

Wang, Y., Okamoto, M., Schmitz, F., Hofmann, K., and Südhof, T.C. (1997). Rim is a putative Rab3 effector in regulating synaptic-vesicle fusion. Nature *388*, 593–598.

Way, J.C., and Chalfie, M. (1989). The *mec-3* gene of *Caenorhabditis elegans* requires its own product for maintained expression and is expressed in three neuronal cell types. Genes Dev. *3*, 1823–1833.

White, J.G., Southgate, E., Thomson, J.N., and Brenner, S. (1986). The structure of the nervous system of *Caenorhabditis elegans*. Philos. Trans. R. Soc. Lond. B Biol. Sci. *314*, 1–340.

Williams, B.D., Schrank, B., Huynh, C., Shownkeen, R., and Waterston, R.H. (1992). A genetic mapping system in *Caenorhabditis elegans* based on polymorphic sequence-tagged sites. Genetics *131*, 609–624.

Yuan, J., Tirabassi, R.S., Bush, A.B., and Cole, M.D. (1998). The C. elegans MDL-1 and MXL-1 proteins can functionally substitute for vertebrate MAD and MAX. Oncogene *17*, 1109–1118.

Zhao, H., and Nonet, M.L. (2000). A retrograde signal is involved in activity-dependent remodeling at a *C. elegans* neuromuscular junction. Development, in press.

Zhen, M., Huang, X., Bamber, B., and Jin, Y. (2000). Regulation of presynaptic terminal organization by *C. elegans* RPM-1, a putative guanine nucleotide exhanger with a RING-H2 finger domain. Neuron *26*, this issue, 331–343.